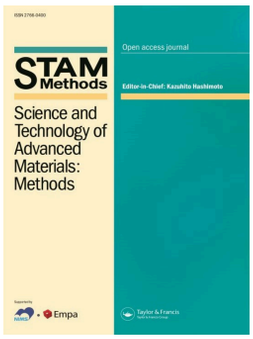

Science and Technology of Advanced Materials: Methods

ISSN: 2766-0400 (Online) Journal homepage: www.tandfonline.com/journals/tstm20

Development of soft X-ray microscope with a four-pole magnet

Yuta Ishii, Yusuke Kozuka, Shiro Kawachi, Toshimitsu Ito, Yusuke Wakabayashi, Hironori Nakao, Taka-Hisa Arima & Yuichi Yamasaki

To cite this article: Yuta Ishii, Yusuke Kozuka, Shiro Kawachi, Toshimitsu Ito, Yusuke Wakabayashi, Hironori Nakao, Taka-Hisa Arima & Yuichi Yamasaki (2025) Development of soft X-ray microscope with a four-pole magnet, Science and Technology of Advanced Materials: Methods, 5:1, 2586300, DOI: 10.1080/27660400.2025.2586300

To link to this article: https://doi.org/10.1080/27660400.2025.2586300

Published online: 02 Dec 2025.

SCIENCE AND TECHNOLOGY OF ADVANCED MATERIALS: METHODS
2025, VOL. 5, NO. 1, 2586300
https://doi.org/10.1080/27660400.2025.2586300

Development of soft X-ray microscope with a four-pole magnet

Yuta Ishii[a,b], Yusuke Kozuka[c,d], Shiro Kawachi[e], Toshimitsu Ito[f], Yusuke Wakabayashi[g], Hironori Nakao[h], Taka-Hisa Arima[i,j] and Yuichi Yamasaki[a,i,k]

[a]Center for Basic Research on Materials (CBRM), National Institute for Materials Science (NIMS), Tsukuba, Japan; [b]PRESTO, Japan Science and Technology Agency (JST), Kawaguchi, Japan; [c]Research Center for Materials Nanoarchitectonics (MANA), National Institute for Materials Science (NIMS), Tsukuba, Japan; [d]WPI Advanced Institute for Materials Research, Tohoku University, Sendai, Japan; [e]Graduate School of Science, University of Hyogo, Koto, Hyogo, Japan; [f]Core Electronics Technology Research Institute (CETRI), National Institute of Advanced Industrial Science and Technology (AIST), Tsukuba, Japan; [g]Department of Physics, Graduate School of Science, Tohoku University, Sendai, Japan; [h]Photon Factory, Institute of Materials Structure Science, High Energy Accelerator Research Organization (KEK), Tsukuba, Japan; [i]Center for Emergent Matter Science (CEMS), RIKEN, Wako, Japan; [j]Department of Advanced Materials Science, The University of Tokyo, Kashiwa, Japan; [k]International Center for Synchrotron Radiation Innovation Smart, Tohoku University, Sendai, Japan

ABSTRACT

Soft X-ray microscopic experiments, such as scanning X-ray microscopy (SXM) and coherent X-ray imaging (CDI), have emerged as powerful techniques for investigating magnetic materials. However, X-ray imaging experiments under external magnetic fields with flexible orientation remain limited. We have developed a soft X-ray microscope equipped with a four-pole electromagnet, enabling imaging experiments magnetic field orientations continuously adjustable from parallel to perpendicular to the incident X-ray beam. This unique capability allows versatile experimental configurations, facilitating static magnetic imaging and advanced time-resolved imaging. We performed time-resolved SXM measurements on two different types of NiFe (permalloy) samples, successfully capturing the collective magnetization dynamics induced by ferromagnetic resonance effect. Furthermore, CDI measurement is demonstrated on multiferroic $BiFeO_3$, visualizing sinusoidal magnetic structures with a spatial periodicity on the order of ten nanometers. The results highlight the efficiency of the developed X-ray microscope as a platform for studying the dynamics and complex spin textures of magnetic materials and spintronic devices.

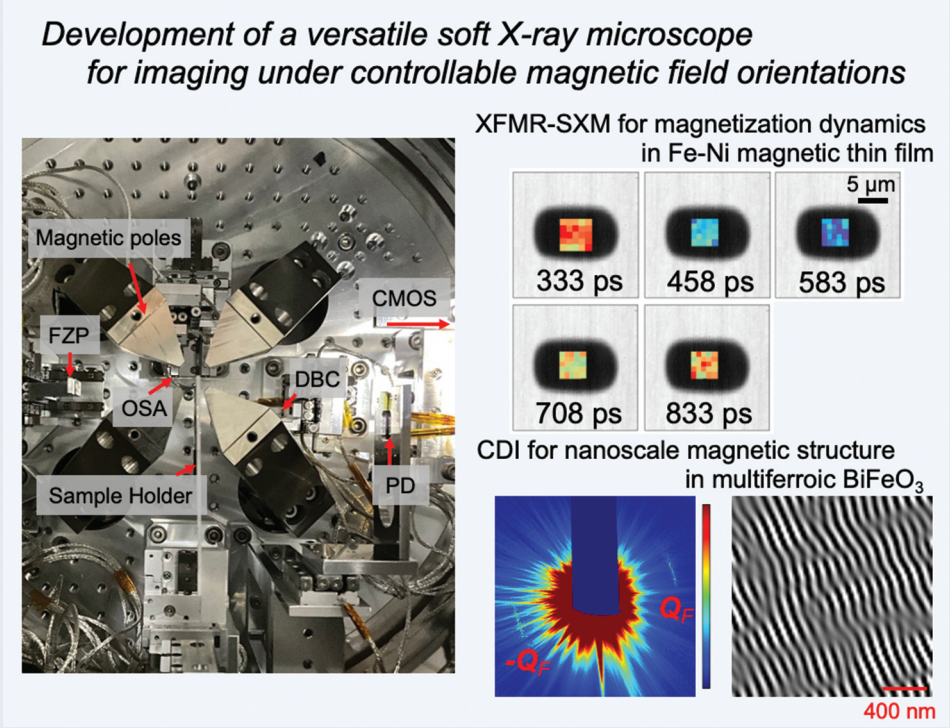

ARTICLE HISTORY
Received 27 August 2025
Revised 29 October 2025
Accepted 3 November 2025

KEYWORDS
X-ray microscope; advanced X-ray imaging

CONTACT Yuta Ishii ISHII.Yuta@nims.go.jp Center for Basic Research on Materials (CBRM), National Institute for Materials Science (NIMS), 1-2-1, Sengen, Tsukuba 305-0047, Japan

IMPACT STATEMENT
We present the development of a soft X-ray microscope with a four-pole electromagnet, enabling versatile magnetic field orientations, and demonstrate advanced measurements for magnetization dynamics and nanoscale magnetic texture.

1. Introduction

Over the past decades, X-ray imaging techniques have been developed significantly, enabling visualization of the structures in several types of materials. Among the various applications of X-ray imaging, one of the most significant areas for soft X-ray is the study of magnetic materials. Soft X-rays, near the absorption edges of 3*d* and 4*f* transition elements, offer resonant experiments including X-ray magnetic circular dichroism (XMCD), X-ray magnetic linear dichroism (XMLD), and resonant X-ray magnetic scattering (RXMS). These techniques provide information on several properties of the specific element such as spin and orbital angular momenta [1–3] and anisotropic magnetic dipole terms (T_z) [4–9]. To combine these resonant measurements with X-ray imaging approaches provide powerful techniques for visualizing nanoscale textures such as ferromagnetic domain [10–13], magnetic skyrmion lattice [14–17], and other complex spin textures in three-dimensional systems [18–20]. Highly coherent and short-pulsed X-rays at synchrotron facilities significantly improve the spatial and time resolutions, paving the way for further development of X-ray imaging, like time-resolved experiments for the dynamics of magnetic moments [21–24].

To address the growing demand for versatile imaging measurements in external magnetic fields, we have developed a soft X-ray microscope equipped with a four-pole electromagnetic coil assembly. In this paper, we present the features of the microscope and demonstrate time-resolved SXM measurements for proving collective magnetization dynamics in $Ni_{0.8}Fe_{0.2}$ (permalloy : Py) and CDI for magnetic structure in multiferroic $BiFeO_3$. The results show the effectiveness of the developed microscope system for advanced soft X-ray imaging of magnetic materials.

2. Instrument for soft X-ray microscopy under magnetic field

Figure 1(a,b) shows the exterior of the soft X-ray microscope and the interior of the vacuum chamber, respectively. The vacuum chamber is placed on the motorized base stage for precise alignment of the chamber center with the X-ray optical axis. All essential components for soft X-ray microscopy including piezo-stages, Fresnel zone plate (FZP), and an order sorting aperture (OSA) are housed within high-vacuum environment of a base pressure of the order of 10^{-6} Pa. A photodiode (PD) detector and a complementary-metal-oxide-semiconductor (CMOS) camera are positioned downstream of the sample to detect X-rays transmitted through or scattered by the sample. This configuration enables several types of imaging techniques, like SXM, holography, CDI, and ptychography. Furthermore, a sub-miniature-type-A (SMA) cable is introduced into the vacuum chamber and connected to the sample holder to apply electric current, voltage, and microwave signals to the sample to perform a variety of operando measurements.

In this system, electromagnets are employed in consideration of both the need for a compact magnetic field generation setup that is compatible with the microscopic optical components and the requirement for variable and controllable magnetic field strength. As seen in Figure 1(a), four electromagnetic coils are installed outside and beneath the vacuum chamber, and magnetic flux is guided into the sample region through a four-pole magnetic circuit [see 'Magnetic poles' in Figure 1(b)]. The usable sample area spans nearly 5 mm × 5 mm. When an electric current of 2.5 A is supplied to the electromagnetic coils, a maximum field of approximately 600 mT is generated. The spatial variation of the magnetic field is approximately 0.5 mT over 10 μm when a magnetic field of 500 mT is applied, determined by electromagnetic field simulations. Figure (c) shows the magnetic field amplitude in the vicinity of the sample position when the central field amplitude is 500 mT. This configuration enables the magnetic field orientation to be continuously varied between parallel and perpendicular to the incident X-ray beam. Figure 2(a,b) illustrates the cases that the magnetic field $\mathbf{H}$ is parallel and perpendicular to the wavevector $\mathbf{k}_i$ of the incident X-rays ($\mathbf{H} \parallel \mathbf{k}_i$ and $\mathbf{H} \perp \mathbf{k}_i$), respectively. Under the geometry of $\mathbf{H} \parallel \mathbf{k}_i$, conventional XMCD measurements can be performed, as illustrated in Figure 2(c). A representative XMCD spectrum is shown in Figure 2(e). The data are acquired with the X-ray transmission through a 30 nm-thick Py thin film around the Ni $L_{2,3}$ absorption edges. In contrast, the $\mathbf{H} \perp \mathbf{k}_i$ configuration is effective for XFMR experiments, as described below.

3. Time-resolved scanning X-ray microscopy for studying magnetization dynamics

As a practical application of X-ray imaging under an external magnetic field, we present a time-resolved SXM technique utilizing our microscope to probe the collective dynamics of magnetic moments. Recent decades, time-resolved XMCD methods have been

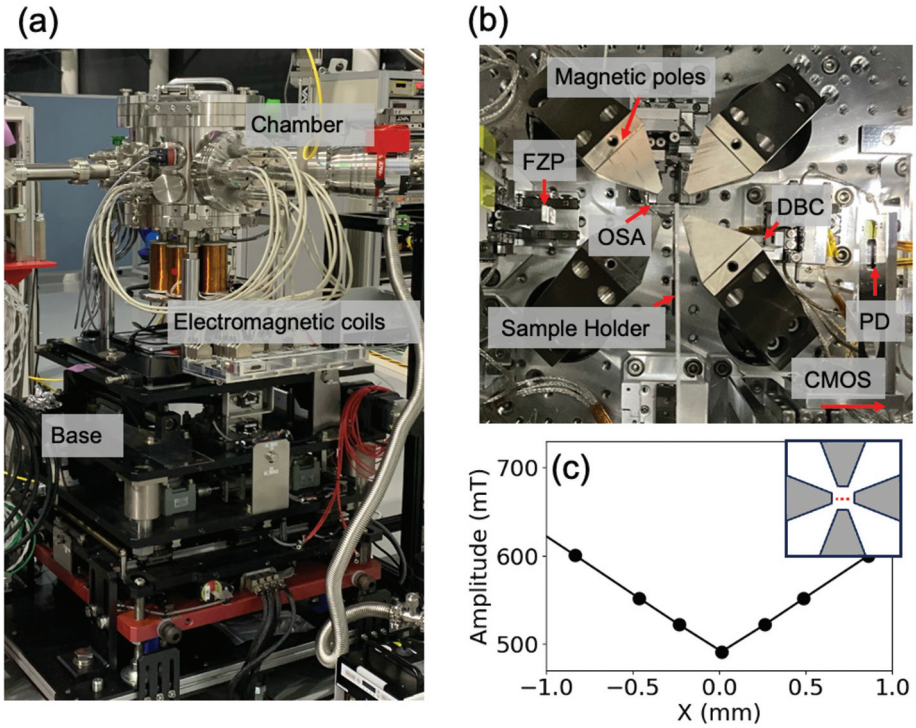

Figure 1. (a) Appearance of the soft X-ray microscope and (b) internal configuration of the vacuum chamber. FZP, OSA, DBC, and PD denote fresnel zone plate, order sorting aperture, direct beam catcher, and photo diode, respectively. A CMOS camera is installed outside the chamber. (c) Magnetic field amplitude near the sample position, obtained from electromagnetic field simulations, plotted along the direction from one magnetic Pole to its counterpart as indicated by the red doted line in the inset.

advanced to enable real-time observation of magnetization dynamics under the ferromagnetic resonance (FMR) effect, where the precession of magnetic moments is induced by externally applied gigahertz (GHz)-microwave [21–24]. This technique, known as X-ray ferromagnetic resonance (XFMR), has been successfully applied for various magnetic systems.

Typical XFMR geometry under the configuration $\mathbf{H}\perp\mathbf{k}_i$ is illustrated in Figure 2(d). The sample is placed on an electrode, and an alternating current (AC) is introduced through the electrode, producing an AC magnetic field ($\mathbf{h}^{AC}$) around the sample. A static magnetic field $\mathbf{H}$ is applied perpendicular to both $\mathbf{h}^{\mathrm{AC}}$ and $\mathbf{k}_i$. This $\mathbf{H}$ and $\mathbf{h}^{\mathrm{AC}}$ configuration excites magnetization precession via FMR effect. In XFMR experiments, $\mathbf{h}^{\mathrm{AC}}$ is usually tuned to harmonics of the X-ray injection frequency. By incrementally delaying the phase of $\mathbf{h}^{\mathrm{AC}}$ with respect to the timing of X-ray injection, XMCD signals are recorded at each delay time. Through this time-resolved detection, the X-ray beam probes the precessional dynamics of the magnetization, specifically its components parallel to $\mathbf{k}_i$, which is referred to as the XFMR signal. This measurement provides information on magnetization dynamics. Comprehensive details regarding the XFMR system that we developed can be found in our prior publication [24]. Representative XFMR data acquired from a Py microstructure at the Ni L_3 edge is presented in Figure 2(f) (The details of the sample are mentioned below). The experiments were performed at BL-16A of Photon Factory (PF), High Energy Accelerator Research Organization (KEK), Japan. The $\mathbf{H}$ amplitude is 6 mT, while 2.0 GHz $\mathbf{h}^{\mathrm{AC}}$ is applied to the sample. Distinct oscillatory signals with a 500-ps periodicity, corresponding to the $\mathbf{h}^{\mathrm{AC}}$ frequency, are observed. The red dashed line in the figure represents fitting results of a sinusoidal function with a frequency of 2.0 GHz to the experimental result.

3.1. Detection of uniform spin precession in microstructured permalloy

Combining XFMR with X-ray imaging techniques enables direct visualization of collective magnetization dynamics, such as spin-wave propagation [22,23,25–33]. Here, we demonstrate the integration of XFMR and SXM measurements, herein referred to as XFMR-SXM, conducted on a microstructured Py sample. The experimental setup is depicted in Figure 3(a). The sample was fabricated using photolithography and positioned on a 30-nm-thick Au electrode line deposited on a SiN membrane via sputtering. The sample was electrically isolated from the electrode by a 100-nm-thick SiO_2 interlayer. The lateral dimensions of the Py structure are approximately 10 μm, with a thickness of 30 nm. A micrograph of the fabricated sample is shown in the inset of Figure 3(a). A circularly polarized X-ray beam is focused by an FZP with outer and center beam-stopper radii of 60 and 30 μm. The higher-order diffractions from

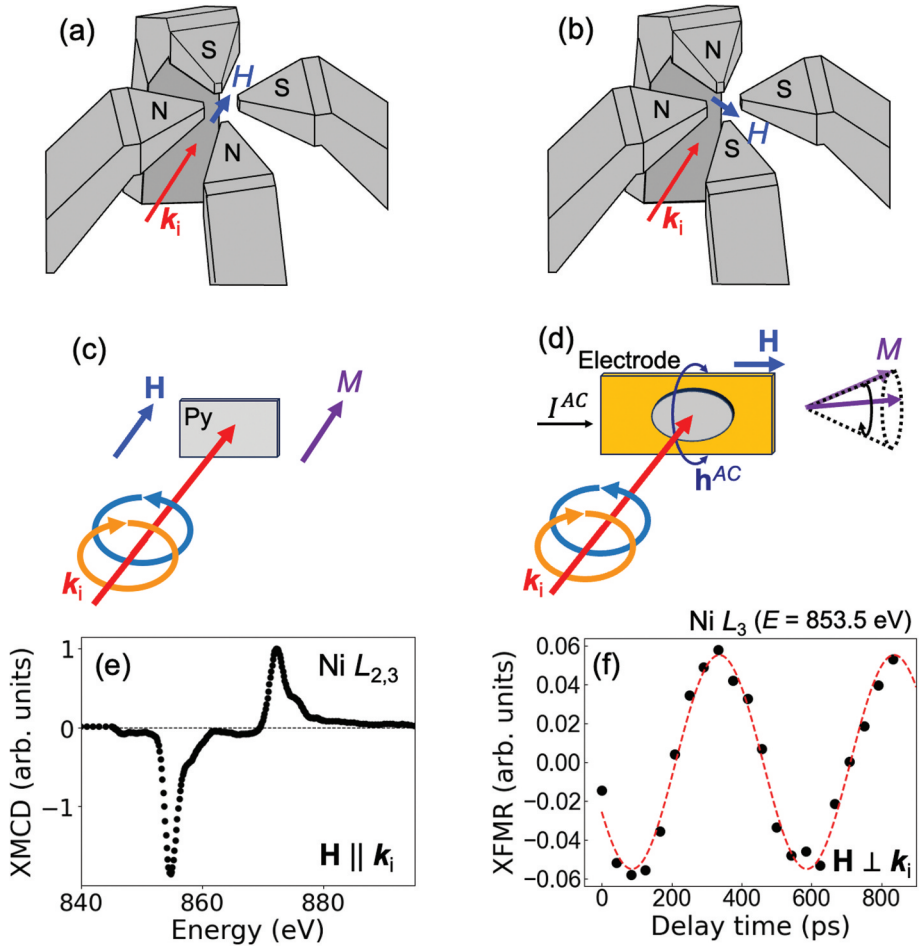

Figure 2. (a,b) Experimental configurations in a four-pole magnetic system: (a) $\mathbf{H} \parallel \mathbf{k}_i$ and (b) $\mathbf{H} \perp \mathbf{k}_i$, where $\mathbf{H}$ and k_i denote the directions of magnetic field and incident X-ray beam, respectively. (c,d) Schematic illustrations of the XMCD and XFMR experimental geometries: (c) XMCD measurement under the condition $\mathbf{H} \parallel \mathbf{k}_i$, where the magnetization vector (M) aligns along the magnetic field direction. (d) XFMR setup with $\mathbf{H} \perp \mathbf{k}_i$, where an alternating current (AC) is applied through an electrode, generating an AC magnetic field ($\mathbf{h}^{AC}$) around the sample. The static magnetic field is oriented perpendicular to both $\mathbf{h}^{AC}$ and $\mathbf{k}_i$. This arrangement of $\mathbf{H}$ and $\mathbf{h}^{AC}$ excites magnetization precession through the FMR effect. By sweeping a phase delay of $\mathbf{h}^{AC}$ with respect to the incident X-ray injection, the X-ray beam probes the components of M parallel to the $\mathbf{k}_i$ at each delay time via XMCD detection. (e) XMCD spectrum obtained around the Ni $L_{2,3}$ edges for a 30 nm-thick Py film. An external magnetic field of 250 mT is applied parallel to the incident X-ray direction and normal to the sample surface. (e) Representative XFMR data acquired from a micro-patterned Py structure at the Ni L_3 edge (E = 853.5 eV) (see also Figure 3(a)). A frequency of $\mathbf{h}^{AC}$ is set to 2.0 GHz, and $\mathbf{H}$ is maintained at an amplitude of 6.0 mT. Dashed red line present the fitting of a sinusoidal function with a frequency of 2.0 GHz.

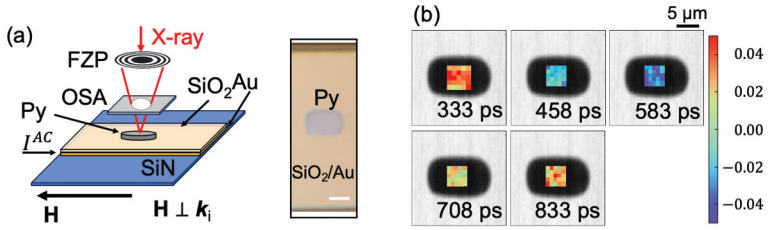

Figure 3. (a) Experimental setup of the XFMR-SXM measurement for a micro-patterned Py structure. The elliptical Py micro-structure is deposited on the Au electrode. A 100 nm-thick SiO_2 layer electrically isolates the Py structure from the electrode. The external magnetic field is applied perpendicular to the incident X-ray direction. The inset displays an optical micrograph of the sample with a scale bar of 10 μm. (b) Spatially resolved XFMR signals as a function of delay time. The contour map presents the spatial distribution of XFMR signals across the sample, overlaid on the SXM image which shows the distribution of the transmitted intensity from the sample.

the FZP are filtered by an OSA with a radius of 10 μm. In this measurement, the beam size at focal point is approximately 500 nm. The sample is precisely placed at the focal point of the FZP. Spatially resolved maps of the XFMR signal intensity in the central area of the sample are presented in Figure 3(b), where the XFMR intensities are overlaid on the SXM image which shows the distribution of the transmitted intensity from the sample. Due to substantial soft X-ray attenuation by the Py, the SiO_2 insulating layer, and the underlying electrode, the transmitted X-ray intensity is reduced by an order of magnitude (10^{-1}). Nevertheless, a nearly uniform precession of magnetic moments, which can be characterized by the Kittel spin-wave mode, is observed. This result demonstrates a successful detection of spin-waves excited in a microstructured magnetic sample.

3.2. Detection of nonreciprocal spin-wave propagation

XFMR-SXM measurement can also be employed to detect spin waves with finite wavelengths. Figure 4(a) illustrates the experimental configuration for the detection of finite-wavelength spin-waves in a Py thin film, fabricated by sputtering over an electrode with a width of 10 μm. I^{AC} with a frequency of 4.0 GHz is supplied to the electrode. Under this configuration, magnetostatic surface spin waves (MSSWs), excited by the applied I^{AC}, propagate bidirectionally along the z axis defined in the figure. Figure 4(b) presents the X-ray transmission intensity distribution in the vicinity of the electrode. The focused X-ray beam detected XFMR signals at positions A and B, as marked in the figure. Figure 4(c,d) displays the delay-time dependence of the XFMR signals acquired at these positions under an external magnetic field $H = \pm 30$ mT. The amplitudes and phases of the oscillatory XFMR signals at positions A and B exhibit notable differences. The amplitude and phase ratios between these two positions are inverted upon reversal of the applied magnetic field. These results are indicative of the nonreciprocity of the amplitude and wavelength of MSSWs. This nonreciprocal behavior arises from directional asymmetry of the external magnetic field at the positions A and B, in addition to the unequal magnetic anisotropies at the opposing surfaces of the thin film [34,35]. Ongoing investigations focus on further elucidating this nonreciprocity.

3.3. Coherent soft X-ray diffraction imaging

A CDI measurement for a nanoscale magnetic structure of a multiferroic $BiFeO_3$ is demonstrated as another advanced application of the developed microscope employing the RXMS technique. In comparison with SXM measurements, CDI enables higher spatial-resolution imaging down to 10-nanometre scale.

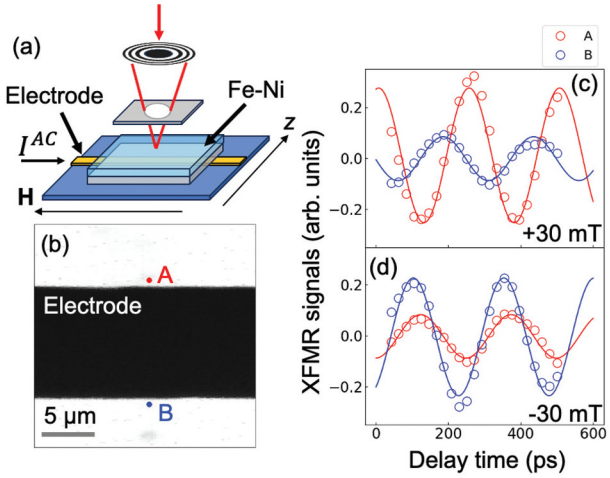

Figure 4. (a) Experimental configuration of the XFMR-SXM measurement for finite-wavelength spin-wave detection. (b) SXM image near the Au electrode, with a scale bar indicating 5 μm. (c,d) XFMR signals acquired at positions A and B under external magnetic fields of $H = \pm 30$ mT. Red and blue curves correspond to the fitted results.

$BiFeO_3$ is a room-temperature multiferroic material exhibiting a large spontaneous polarization of approximately 90 $\mu C/cm^2$, a high Curie temperature of ~1100 K, and approximately G-type antiferromagnetic order with the Néel temperature of ~653 K [36]. The antiferromagnetic order is modified by a Dzyaloshinskii-Moriya (DM) interaction between Fe spins to form a sinusoidal magnetic structure with a wavelength of 62 nm [37,38]. The magnetic structure can be described as a superposition of an antiferromagnetic modulation vector $\mathbf{Q}_{AF} = (1 - q_m, 1 + q_m, 1)$ and a spatially modulated weak ferromagnetic component with $\mathbf{Q}_F = (-q_m, q_m, 0)$, where $q_m = 0.0045$. The latter magnetic modulation is detectable with a transmission-mode resonant soft X-ray small-angle scattering (RSXS) setup.

To transmit soft X-rays, the sample was thinned to a thickness of approximately 200 nm using focused ion beam (FIB) processing and mounted on a 10 μm pinhole [see Figure 5(a)]. The pinhole was fabricated by depositing gold onto a Si_3N_4 membrane, followed by FIB milling to open the aperture [14]. Soft X-ray microscopy measurements were conducted at beamline BL14U of NanoTerasu, and the diffraction patterns were recorded using a Complementary Metal-Oxide-Semiconductor (CMOS) camera. Figure 5(b) shows the X-ray absorption spectrum (XAS) near the Fe $L_{2,3}$-edge. Based on the spectral shape, the photon energy for magnetic scattering measurements is set to 707.4 eV. The incident X-rays with circular polarization are directed parallel to the $[111]_{rh}$ direction, where $[\cdots]_{rh}$ denotes the rhombohedral lattice index. Figure 5(c) presents the coherent diffraction pattern, where magnetic scattering from the sinusoidal magnetic structure is observed. Fraunhofer diffraction from the pinhole appears around the center of the pattern and interferes with the magnetic scattering signals. The

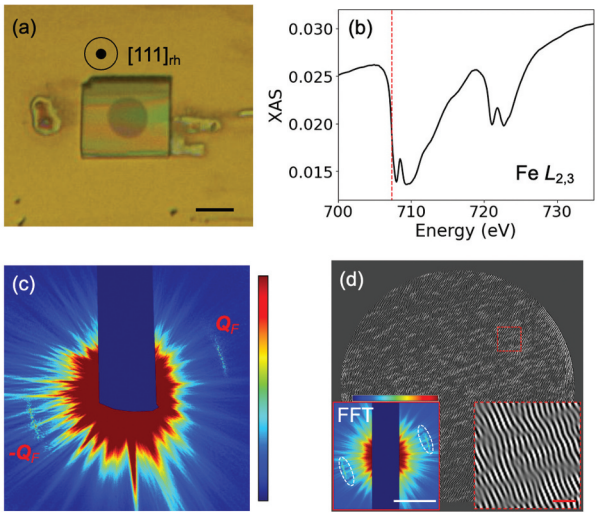

Figure 5. (a) Optical micrograph of a flake-shaped $BiFeO_3$ single crystal mounted on a pinhole with a diameter of 10 μ m. The sample thickness is approximately 200 nm. The scale bar corresponds to 10 μm. (b) X-ray absorption spectrum near the Fe $L_{2,3}$ absorption edges. The dashed line indicates 707.4 eV, the energy at which the cdi measurement is conducted. (c) Coherent X-ray diffraction pattern for weak ferromagnetic scattering. (d) Reconstructed real-space image of the sinusoidal magnetic structure after frequency filtering. The left inset shows the fft image of the reconstructed real-space structure, with the central area masked. The dashed ellipses indicate the windows for frequency filtering. The scale bar represents 0.1 nm^{-1}. The right inset presents an enlarged view of the region delineated by a red dashed line in the figure. The scale bar corresponds to 400 nm.

Hybrid Input-Output (HIO) phase retrieval analysis [39] is applied to the diffraction pattern shown in Figure 5(c). To further enhance the discernibility of the magnetic structure, frequency filtering was subsequently employed on the reconstructed image to extract the $\mathbf{Q}_F$ frequency component. The resulting magnetic structure, obtained through this procedure, is presented in Figure 5(d). The right inset of Figure 5(d) shows the FFT image of the reconstructed real-space structure, where dashed ellipses indicate the windows used for frequency filtering. As shown in Figure 5(d), the spatially modulated component of the ferromagnetic moment is successfully visualized. Although no clear magnetic-field effect on the magnetic structure is observed in the present setup, the results demonstrate that the magnetic imaging capability was sufficiently evaluated. By integrating this technique with the dynamic measurements discussed in the previous sections, time-resolved magnetic imaging is expected to become feasible in the future.

4. Conclusion

We have developed a soft X-ray microscopy system with a four-pole electromagnet, enabling advanced imaging measurements under external magnetic fields with flexible directional control, significantly expanding the range of experimental geometries for soft X-ray imaging. We have successfully conducted time-resolved XFMR-SXM on spin waves in Py samples. Furthermore, real-space imaging for the magnetic structure in multiferroic $BiFeO_3$ is achieved by a CDI measurement. These results demonstrate the capability of direct visualization of magnetic systems. Our results underscore the utility of this newly developed microscope as a versatile platform for studying static and dynamic magnetic phenomena at nanoscale. It opens up new opportunities for investigating spintronic devices, magnetic thin films, and complex spin textures with high spatial and time resolution.

Acknowledgements

Time-resolved SXM and CDI measurement were performed at BL-16A of Photon Factory (PF), High Energy Accelerator Research Organization (KEK), Tsukuba, Japan, and BL14U of NanoTerasu, Sendai, Japan, respectively. We thank Tetsuya Nakamura, Yoshinori Kotani, Akiho Sumiyoshiya, Yusuke Tanimoto, and Taishi Kawabata at PhoSIC for supporting us with the CDI experiments at NanoTerasu. Soft X-ray experiments at PF were performed under the approval of the Photon Factory Program Advisory Committee (Proposal Nos. 2018S2-006, 2019G590, 2019PF-22, 2021PF-S003, 2021S2-004, and 2021G691). This work was supported by Advanced Research Infrastructure for Materials and Nanotechnology in Japan (ARIM) of the Ministry of Education, Culture, Sports, Science and Technology (MEXT). Proposal Number JPMXP1224NM5558 and JPMXP1225NM5403. MANA and AIMR are supported by World Premier International Research Center Initiative (WPI), MEXT, Japan.

Disclosure statement

No potential conflict of interest was reported by the author(s).

Funding

This work was partially supported by JSPS KAKENHI [Project Nos. JP19K23590, JP19H04399, JP20K20107, JP23K17145, JP24K03205, JP24H01685, JP25K03387], by PRESTO [JPMJPR2102] and CREST [JPMJCR1861 and JPMJCR2435] Japan Science and Technology Agency (JST). This work was supported by MEXT Quantum Leap Flagship Program (MEXT Q-LEAP) [Grant Number JPMXS0118068681].

ORCID

Yuta Ishii http://orcid.org/0000-0002-8957-5833
Yuichi Yamasaki http://orcid.org/0000-0002-8560-3462

References

[1] Carra P, Thole BT, Altarelli M, et al. X-ray circular dichroism and local magnetic fields. Phys Rev Lett. 1993 Feb;70(5):694–697. doi: 10.1103/PhysRevLett.70.694

[2] Chen CT, Idzerda YU, Lin H, et al. Experimental confirmation of the X-ray magnetic circular dichroism sum rules for iron and cobalt. Phys Rev Lett. 1995 Jul;75(1):152–155. doi: 10.1103/PhysRevLett.75.152

[3] Laan G. Angular momentum sum rules for x-ray absorption. Phys Rev B. 1998;57(1):112–115. doi: 10.1103/PhysRevB.57.112

[4] Yamasaki Y, Nakao H, Arima TH. Augmented magnetic octupole in kagomé 120-degree antiferromagnets detectable via X-ray magnetic circular dichroism. J Phys Soc Jpn. 2020 Aug;89(8):083703. doi: 10.7566/JPSJ.89.083703

[5] Kimata M, Sasabe N, Kurita K, et al. X-ray study of ferroic octupole order producing anomalous Hall effect. Nat Commun. 2021 Sep;12(1):5582. doi: 10.1038/s41467-021-25834-7

[6] Sakamoto S, Higo T, Shiga M, et al. Observation of spontaneous x-ray magnetic circular dichroism in a chiral antiferromagnet. Phys Rev B. 2021 Oct;104(13):134431. doi: 10.1103/PhysRevB.104.134431

[7] Sasabe N, Mizumaki M, Uozumi T, et al. Ferroic order for anisotropic magnetic dipole term in collinear antiferromagnets of $(t_{2g})^4$ system. Phys Rev Lett. 2023 Nov;131(21):216501. doi: 10.1103/PhysRevLett.131.216501

[8] Koizumi H, Yamasaki Y, Yanagihara H. Quadrupole anomalous Hall effect in magnetically induced electron nematic state. Nat Commun. 2023 Dec;14(1):8074. doi: 10.1038/s41467-023-43543-1

[9] Yamasaki Y, Ishii Y, Sasabe N. Sum rules for x-ray circular and linear dichroism based on complete magnetic multipole basis. Sci Technol Adv Mater. 2025;26(1):2513217. doi: 10.1080/14686996.2025.2513217

[10] Ukleev V, Yamasaki Y, Morikawa D, et al. Element-specific soft x-ray spectroscopy, scattering, and imaging studies of the skyrmion-hosting compound $Co_8Zn_8Mn_4$. Phys Rev B. 2019 Apr;99(14):144408. doi: 10.1103/PhysRevB.99.144408

[11] Ishii Y, Nakao H, Mizumaki M, et al. Topological charge of soft x-ray vortex beam determined by inline holography. Sci Rep. 2022;12(1):1044. doi: 10.1038/s41598-022-04933-5

[12] Ishii Y, Kozuka Y, Yamasaki Y, et al. Development of multi-scale soft x-ray diffraction microscope for observing spin textures. In: Proceedings of the 29th International Conference on Low Temperature Physics (LT29), JPS Conf. Proc., Sapporo, Japan; 2023. Vol. 38. p. 01190.

[13] Battistelli R, Metternich D, Schneider M, et al. Coherent x-ray magnetic imaging with 5 nm resolution. Optica. 2024 Feb;11(2):234–237. doi: 10.1364/OPTICA.505999

[14] Yamasaki Y, Morikawa D, Honda T, et al. Dynamical process of skyrmion-helical magnetic transformation of the chiral-lattice magnet FeGe probed by small-angle resonant soft X-ray scattering. Phys Rev B. 2015 Dec;92(22):220421. doi: 10.1103/PhysRevB.92.220421

[15] Ukleev V, Yamasaki Y, Morikawa D, et al. Coherent resonant soft x-ray scattering study of magnetic textures in FeGe. Quantum Beam Sci. 2018;2(1):3. doi: 10.3390/qubs2010003

[16] Ishii Y, Yamamoto K, Yokoyama Y, et al. Soft-x-ray vortex beam detected by inline holography. Phys Rev Appl. 2020 Dec;14(6):064069. doi: 10.1103/PhysRevApplied.14.064069

[17] Birch MT, Powalla L, Wintz S, et al. History-dependent domain and skyrmion formation in 2D van der Waals magnet Fe_3GeTe_2. Nat Commun. 2022;13(1):3035. doi: 10.1038/s41467-022-30740-7

[18] Hierro-Rodriguez A, Quirós C, Sorrentino A, et al. Revealing 3D magnetization of thin films with soft x-ray tomography: magnetic singularities and topological charges. Nat Commun. 2020;11(1):6382. doi: 10.1038/s41467-020-20119-x

[19] Donnelly C, Hierro-Rodrguez A, Abert C, et al. Complex free-space magnetic field textures induced by three-dimensional magnetic nanostructures. Nat Nanotechnol. 2022;17(2):136–142. doi: 10.1038/s41565-021-01027-7

[20] Rana A, Liao CT, Iacocca E, et al. Three-dimensional topological magnetic monopoles and their interactions in a ferromagnetic meta-lattice. Nat Nanotechnol. 2023;18(3):227–232. doi: 10.1038/s41565-022-01311-0

[21] Finizio S, Wintz S, Zeissler K, et al. Dynamic imaging of the delay- and tilt-free motion of Néel domain walls in perpendicularly magnetized superlattices. Nano Lett. 2019 01;19(1):375–380. doi: 10.1021/acs.nanolett.8b04091

[22] Gräfe J, Gruszecki P, Zelent M, et al. Direct observation of spin-wave focusing by a Fresnel lens. Phys Rev B. 2020 07;102(2):024420. doi: 10.1103/PhysRevB.102.024420

[23] Girardi D, Finizio S, Donnelly C, et al. Three-dimensional spin-wave dynamics, localization and interference in a synthetic antiferromagnet. Nat Commun. 2024;15(1):3057. doi: 10.1038/s41467-024-47339-9

[24] Ishii Y, Yamasaki Y, Kozuka Y, et al. Microscopic evaluation of spin and orbital moment in ferromagnetic resonance. Sci Rep. 2024;14(1):15504. doi: 10.1038/s41598-024-66139-1

[25] Stoll H, Puzic A, van Waeyenberge B, et al. High-resolution imaging of fast magnetization dynamics in magnetic nanostructures. Appl Phys Lett. 2004 [2023 01 11];84(17):3328–3330. doi: 10.1063/1.1723698

[26] Van Waeyenberge B, Puzic A, Stoll H, et al. Magnetic vortex core reversal by excitation with short bursts of an alternating field. Nature. 2006;444(7118):461–464. doi: 10.1038/nature05240

[27] Noske M, Gangwar A, Stoll H, et al. Unidirectional sub-100-ps magnetic vortex core reversal. Phys Rev B. 2014 09;90(10):104415. doi: 10.1103/PhysRevB.90.104415

[28] Bonetti S, Kukreja R, Chen Z, et al. Direct observation and imaging of a spin-wave soliton with *p*-like symmetry. Nat Commun. 2015;6(1):8889. doi: 10.1038/ncomms9889

[29] Wintz S, Tiberkevich V, Weigand M, et al. Magnetic vortex cores as tunable spin-wave emitters. Nat Nanotechnol. 2016;11(11):948–953. doi: 10.1038/nnano.2016.117

[30] Förster J, Wintz S, Bailey J, et al. Nanoscale x-ray imaging of spin dynamics in yttrium iron garnet. J Appl Phys. 2019 [cited 2023 Jan 11];126(17):173909. doi: 10.1063/1.5121013

[31] Förster J, Gräfe J, Bailey J, et al. Direct observation of coherent magnons with suboptical wavelengths in a single-crystalline ferrimagnetic insulator. Phys Rev B. 2019 12;100(21):214416. doi: 10.1103/PhysRevB.100.214416

[32] Sluka V, Schneider T, Gallardo RA, et al. Emission and propagation of 1D and 2D spin waves with nanoscale wavelengths in anisotropic spin textures. Nat Nanotechnol. 2019;14(4):328–333. doi: 10.1038/s41565-019-0383-4

[33] Donnelly C, Finizio S, Gliga S, et al. Time-resolved imaging of three-dimensional nanoscale magnetization dynamics. Nat Nanotechnol. 2020;15(5):356–360. doi: 10.1038/s41565-020-0649-x

[34] Schneider T, Serga AA, Neumann T, et al. Phase reciprocity of spin-wave excitation by a microstrip antenna. Phys Rev B. 2008 Jun;77(21):214411. doi: 10.1103/PhysRevB.77.214411

[35] Gladii O, Haidar M, Henry Y, et al. Frequency non-reciprocity of surface spin wave in permalloy thin films. Phys Rev B. 2016 Feb;93(5):054430. doi: 10.1103/PhysRevB.93.054430

[36] Wang J, Neaton JB, Zheng H, et al. Epitaxial $BiFeO_3$ multiferroic thin film heterostructures. Science. 2003;299(5613):1719–1722. doi: 10.1126/science.1080615

[37] Sosnowska I, Neumaier TP, Steichele E. Spiral magnetic ordering in bismuth ferrite. J Phys C Solid State Phys. 1982 aug;15(23):4835. doi: 10.1088/0022-3719/15/23/020

[38] Sosnowska I, Zvezdin A. Origin of the long period magnetic ordering in BiFeO3. J Magnetism Magnetic Mater. 1995;140–144:167–168. doi: 10.1016/0304-8853(94)01120-6

[39] Fienup JR. Phase retrieval algorithms: a comparison. Appl Opt. 1982 Aug;21(15):2758–2769. doi: 10.1364/AO.21.002758